Increasing the dimensionality of soft microstructures through injection-induced self-folding

Tommaso Ranzani[1,2*], Sheila Russo[1,2], Nicholas W. Bartlett[2], Michael Wehner[2,3], and Robert J. Wood[2]

[1]Department of Mechanical Engineering, Boston University, Boston, MA 02215, USA
[2]Wyss Institute for Biologically Inspired Engineering, Harvard John A. Paulson School of Engineering and Applied Sciences, Harvard University, Cambridge, MA 02138, USA
[3]Department of Computer Engineering, University of California Santa Cruz, Santa Cruz, CA 95064, USA
[*]tranzani@bu.edu

This file includes:

Other Supplementary Materials for this manuscript include the following:

Movies S1 – S6

Supplemental text

Multiple approaches have been proposed in the literature to increase the dimensionality of polymer sheets using a variety of strategies based on anisotropic stress concentrations and use of materials responsive to light, temperature, or humidity, as comprehensively reviewed in[1]. The injection-based self folding method takes advantage of well-established techniques to increase the dimensionality of soft laminates. Using soft lithographic technologies allows us to integrate two dimensional channels paths (that can be transformed into three dimensional networks exploiting laser micro-machining and multilayer bonding methodology) that can be used to selectively activate features in a desired sequence. In addition, this method benefits from the large flexibility in the design space as SU8 patterns can be arbitrarily complex and scalable.

Previous work has demonstrated the possibility of exploiting laser micromachining to release simple soft microactuators from an elastomeric matrix[2]. In addition, fluidic actuators, soft lithography, laser micromachining, lamination, and colored inks in microfluidic networks have been demonstrated previously. However, we believe that this paper presents the first instance of a process that combines the best aspects of each of these into a single, monolithic process. In this work we demonstrate a comprehensive integration of soft lithographic techniques with laser micromachining, where laser micromachining is exploited both for creating three dimensional networks of microchannels embedded in multilayer soft laminates, and to program the motion as well as the bending plane of actuatable features. In addition, through the injection of curable materials we are able to controllably deform predesigned areas of the device, and upon curing of such materials (while the device is in the deformed state), we are able to develop three dimensional structures.

To demonstrate the achievable level of complexity we present the MORPH system: composed of 13 separate soft layers, each with thicknesses varying from 260 to 300 μm, resulting in a completely soft laminate of $\approx$2.8 mm in its flat configuration. Once assembled, the final device has 18 independently controllable DoFs. In our previous work[2], we explored the possibility of combining multiple soft and hard layers to manufacture simple, purely two-dimensional, one DoFs actuators out of a $\approx$2 mm thick laminate. However, this hybrid soft-rigid technique only demonstrated the integration of two soft layers, while having the rest of the laminate composed of hard layers, bonded together using double sided adhesive. Laser cutting, in this case, was mostly used to release the actuators from the soft elastomeric scaffold, rather than to define the plane in which the actuator will move and designing the kinematics of the soft device. Handling, realigning, machining, and bonding multiple, exclusively soft layers is a much more challenging task, entailing basic research and manufacturing questions which require the development of an ad-hoc process. In particular, accuracy and repeatability must be guaranteed throughout the process to realize an intricate 3D microfluidic circuitry through laser machining, realignment, and bonding of soft layers.

With our technique, we can achieve design and topological complexity, as well as functional and structural complexity, that are new to the realm of soft micro devices, paving the way towards achieving similar levels of complexity and functionality as their rigid counterparts[3]. In this paper we look at complexity from different points of view. Here it is defined as the ratio of the largest feature size of a device to the smallest. For example, by this definition most animals have a structural complexity of roughly seven to eight orders of magnitude (from smallest cell organelle to a meter-scale organism) while the best 3D printers can achieve approximately four orders of magnitude in complexity.

While the idea of creating 3D structures from 2D processes has been widely explored in more traditional rigid devices, it still presents considerable challenges in the field of soft robotics and more generally soft devices. The strategy of injecting phase-changing materials provides unique advantages in terms of: a) The possibility to control the shape and location of the deformation. The deformation is driven by the combined effect of the shape of the chamber and the laser cut profile of the actuator. The location of the deformation depends on where the inflatable actuators are positioned. b) The ease in performing and generating the desired level of deformation (simply by stopping the injection and initiating curing). c) The possibility to selectively change mechanical properties: depending on the properties of the injected material once cured, we can tune the resulting mechanical properties of the soft laminate, as reported in the SI, section “Injection with phase-changing materials”.

To design devices using the proposed technique, one can exploit already existing tools from the field of origami design and folding-based techniques[4] in conjunction with well established design methodologies for soft devices using soft lithographic techniques[5,6], and design frameworks conceived to develop complex folded laminate devices[7].

Fabrication and process characterization

In this work we expand the concept of combining soft lithographic techniques with laser micromachining to develop 3D soft structures with arbitrarily complex shape and embedded 3D fluidic networks. Here we provide additional details on the injection-induced self-folding process, focusing on the different steps involved.

The process begins with the manufacture of a patterned elastomeric layer via conventional soft lithography. This layer is then transferred to a flexible yet inextensible substrate that is used as a carrier for further processing steps (Figure 1a). A thin polymeric film is placed on top of the layer to keep it clean during handling and subsequent cutting steps. The carrier is placed into a precision laser micromachining system and, after alignment to fiducials defined during soft lithography, the elastomer is cut according to a secondary pattern (Figure 1b). In this phase, we cut only the elastomer and not the carrier using a laser power of 0.7 W and focusing the laser on the top surface of the soft layer. The laser then cuts holes in the carrier that are to be used for future pin alignment. In order to do this, we focus the laser of the carrier and increase the laser power to

1.2 W. This process is repeated for all layers to be used in the final structure. Adjacent layers are then joined using surface functionalization techniques (in this work we use oxygen plasma treatment) and precision pin alignment (Figure 1c). Selective bonding of consecutive layers can be achieved using masking procedures during the functionalization phase. In this way, we create multilayer laminate devices with embedded features (defined via soft lithography) and arbitrary perimeter geometries (defined via laser micromachining).

In the process of cutting through the elastomer, the laser beam damages a small region surrounding the cut path, altering the elastomer surface to such a degree that it can no longer be bonded by oxygen plasma treatment. After performing quantitative analysis, we concluded that this region of thermal damage extends up to 40 μm away from either side of the beam. Further analysis consisted of quantifying the total distortion produced by our process, and consequently defining a standardized procedure for enacting the corresponding alignment corrections. Distortion errors are introduced by thermal shrinkage of the elastomer, stretching and warping caused by handling the thin elastomeric layers, limitations of the laser micromachining system, as well as bonding. Yet, by making the appropriate corrections in the design, we found that distortion errors could be kept down to 4 μm/mm.

In the paragraphs below we detail the characterization of the main aspects of the fabrication process which are: the injection of phase–changing materials, and the capability of laser cutting soft layers in terms of thermally induced damages and limitations in aligning to embossed features.

Quantitative analysis of minimum cut distance

To quantify the effect of thermal damage from the laser on the functionality of our structures, we fabricated arrays of soft micro-actuators with incrementally smaller and smaller minimum distances between the laser cut path and the actuator features. Each actuator was inflated with colored water from a syringe by hand. A digital pressure gauge immediately recorded the pressure in the line. The pressure was increased slowly until the actuator burst (at which point the maximum pressure was recorded), or until the pressure reached 200 kPa.

In Figure S1 we plot the pressure from the gauge as a function of minimum cut distance. We summarize the data in the plot by grouping distance ranges, which can be seen in the Table S1. In general, we note that above 40 μm all actuators reached the maximum pressure tested, suggesting that laser cut paths should be at least this distance from any feature to avoid leaks.

Distortion and alignment analysis

Laser cutting a profile on top of a soft layer with embossed features fabricated through soft lithography, involves multiple steps which could lead to distortions and misalignments. In particular, sources of distortion could derive from the stretchability of the

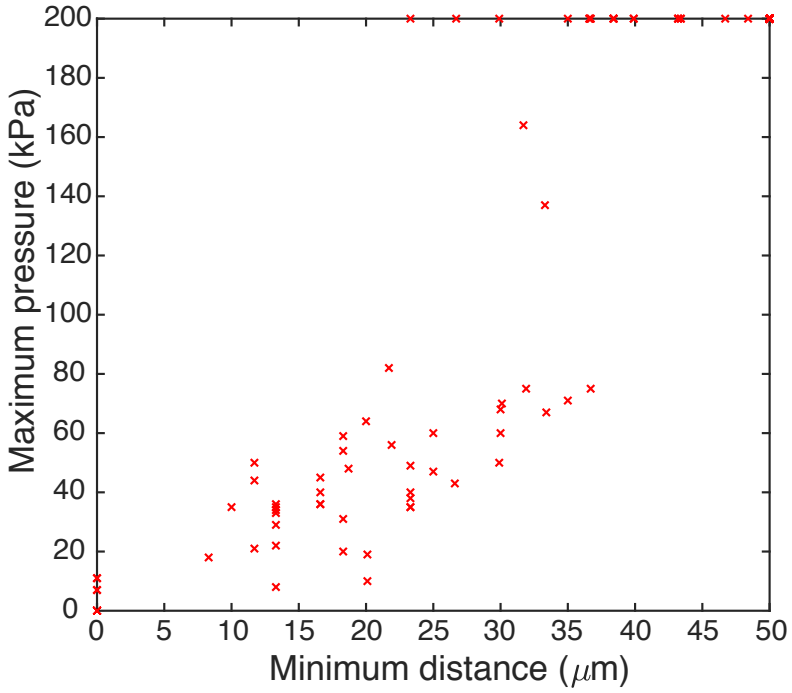

Figure S1. Thermal damage study. Note that actuators that did not leak even at 200 kPa are plotted at 200 kPa.

Distance range (μm)	0 - 10	10 - 20	20 - 30	30 - 40	40+
Average burst pressure (kPa)	1.4	35.9	72.8	158.8	200
% of successful actuators	0	0	18.8	61.1	100
n	39	19	16	18	85

Table S1. "% of successful actuators" refers to actuators that reached the maximum tested pressure of 200 kPa.

soft layers, the alignment process of the layer with respect to the laser micromachining reference system, and the error of the laser cutting system itself.

We analyzed errors deriving from the process by designing a wafer with 17 crosses evenly distributed along the x and y directions within the field of view of the laser cutting system (circumference of 25 mm in diameter). Figure S2a shows the design of the SU-8 pattern on the wafer (white) with the corresponding laser cut path in red.

We prepared a soft layer following the same steps as for the spider and we aligned it to the laser system using three crosses (the central, the farthest on the left and the farthest on the right). Once aligned, we laser cut the path in red (Figure S2a) on top of the existing crosses. We used a confocal microscope (Olympus LEXT OLS4000, Olympus Corporation) to take dimensional data of the actual distance between the embossed crosses to measure the thermal shrinkage due to the polymer curing. Similarly, we measured the error defined as the distance between where the laser cut cross should have been and where it is. The central cross of the soft layer is shown in Figure S2a on the left, demonstrating a perfectly overlapped laser cut cross. Getting to the edges of the layer the error increases and we can see the maximum misalignment for the farthest crosses in the x and

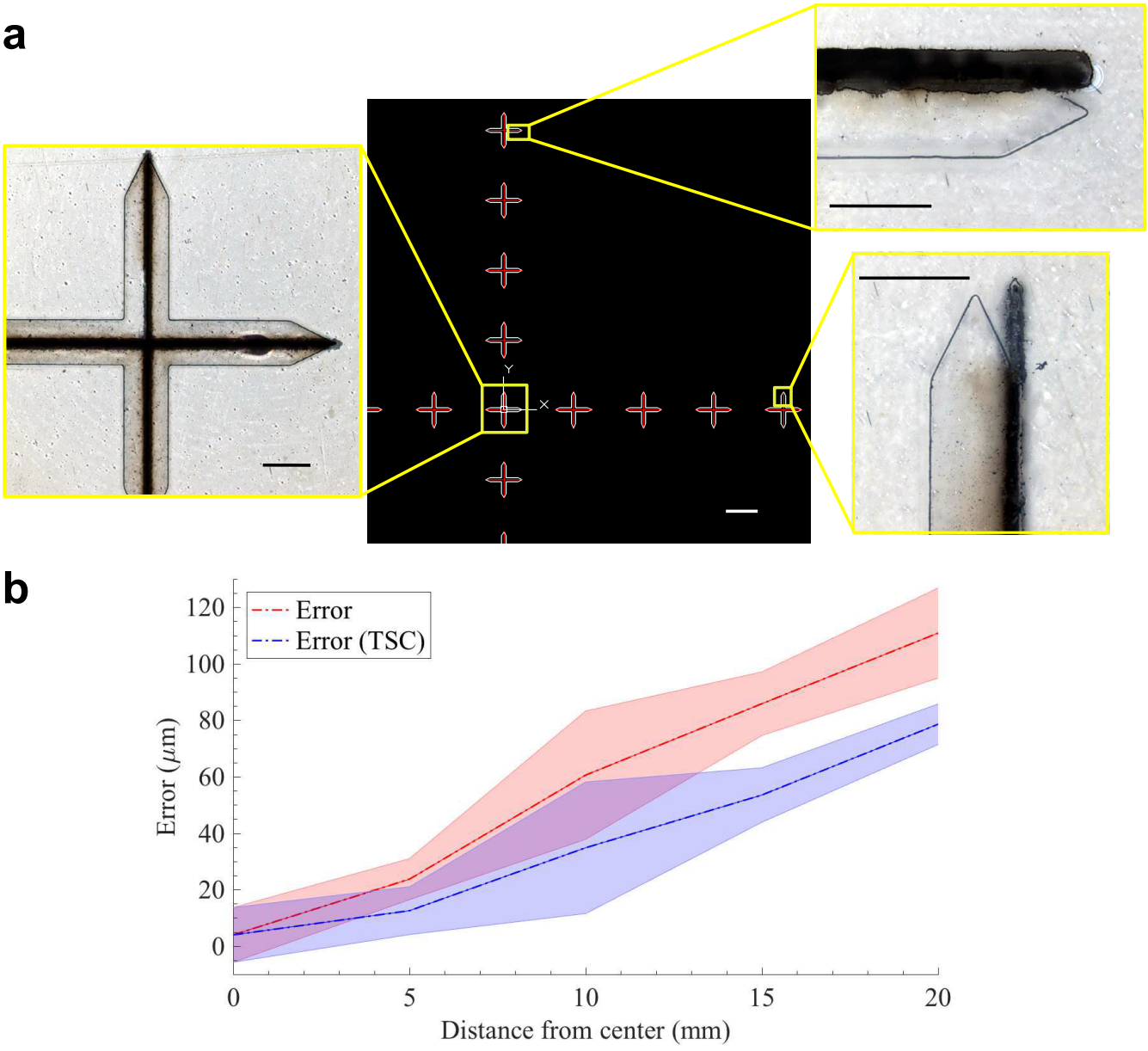

Figure S2. Alignment analysis. a) Crosses arrangement on the wafer in white and in red laser cut path (only one quadrant of the wafer is shown for clarity). Left inset, central cross embossed in the soft layer with the laser cut cross on top of it. Right inset, maximum misalignment in the *y* (top), and *x* (bottom) directions. b) Experimentally measured misalignment distribution along the whole wafer; the case when we compensate for the polymer thermal shrinkage is reported as TSC. Bar scale is 0.3 mm in the left and right insets of a, and it is 5 mm in the center.

y directions highlighted in the right insets of Figure S2a. The error along *x* and *y* for all the crosses was computed and the average is reported in Figure S2b as a function of distance in the wafer. The maximum misalignments are of 111 $\pm 16 \mu$m at 20 mm distance from the center of the layer which results in a 5.6 μm/mm error. By characterizing the thermal shrinkage of the polymers (i.e. measuring the distances between the crosses on the wafer with respect to the distances between the crosses on

Material	Density	Viscosity	Curing Process	Young's Modulus once cured
Sartomer SR355 (90%) and Esacure KTO 46 (10%)	1.01 g/cm3 (SR355)	0.6 Pa s (SR355)	UV	49.5 MPa[8]
Dow Corning Sylgard 184	1.03 g/cm3	3.5 Pa s	Thermal	2.05 MPa[9]
Wacker SilGel 613	0.97 g/cm3	0.15 Pa s	UV	0.01 MPa[10]
Wacker Semicosil 912	0.97 g/cm3	1.00 Pa s	UV	0.005 MPa[11]

Table S2. Phase–changing materials tested.

Material	Elongation at Break	Durometer	Tensile Strength	Young's Modulus
MED4-4220 (NuSil Technology LLC)	580%	17 shore A	4.5 MPa	0.3 MPa
Dow Corning Sylgard 184	140%	43 shore A	6.7 MPa	2.05 MPa[9]

Table S3. Mechanical properties of bulk materials

.

the soft layer), we could compensate for it. In Figure S2b we also show the thermal shrinkage compensated (TSC) error, which is 78.58 $\pm$7.18μm at 20 mm distance from the center, thus resulting in 4 μm/mm error.

Injection with phase–changing materials

We tested the concept of injection with phase–changing materials on simple actuators. We considered materials that cure under different stimuli, that have viscosities up to 3.5 Pa s, and that provide a range of mechanical properties, from a UV curable gel (SilGel 613) to a rigid resin (Sartomer SR355). An overview of the materials tested along with their properties, is reported in Tab. S2. In Figure S3 we show simple soft micro–actuators injected with those materials, in particular Figure S3 a is a spherical actuator injected with UV curable silicone elastomer (Wacker Semicosil 912), Figure S3 b and c show bending actuators injected with the UV curable resin (Sartomer SR355 (90%) and Esacure KTO 46 (10%)), and UV curable silicone gel (Wacker SilGel 613) respectively.

In Figure S4 we can see a bending actuator injected with Sylgard 184, mixed with a red dye for better visualization, which was thermally cured inside the actuator at 60°C for 1 h. We imaged the actuator with a confocal microscope (Olympus LEXT OLS4000, Olympus Corporation). In the inset of Figure S4, we can appreciate the laser cut edges of the two layers composing the actuator as well as the area that is not bonded due to the thermal damage during the laser cutting process (indicated with arrows). We injected some of the legs sublaminates with UV curable resin (Sartomer SR355 (90%) and Esacure KTO 46 (10%)) to demonstrate the fabrication of more complex 3D structures (Figure S5). In this case, the injection of a more rigid material results in a sort of an inner skeleton. In video S3 the injection and curing of the resin in shown. The use of the phase-changing materials allows us to generate a range of mechanical properties in the final structure depending on the material injected. Interfacial mechanic failure is a risk especially when using stiffer and more brittle materials. However, if

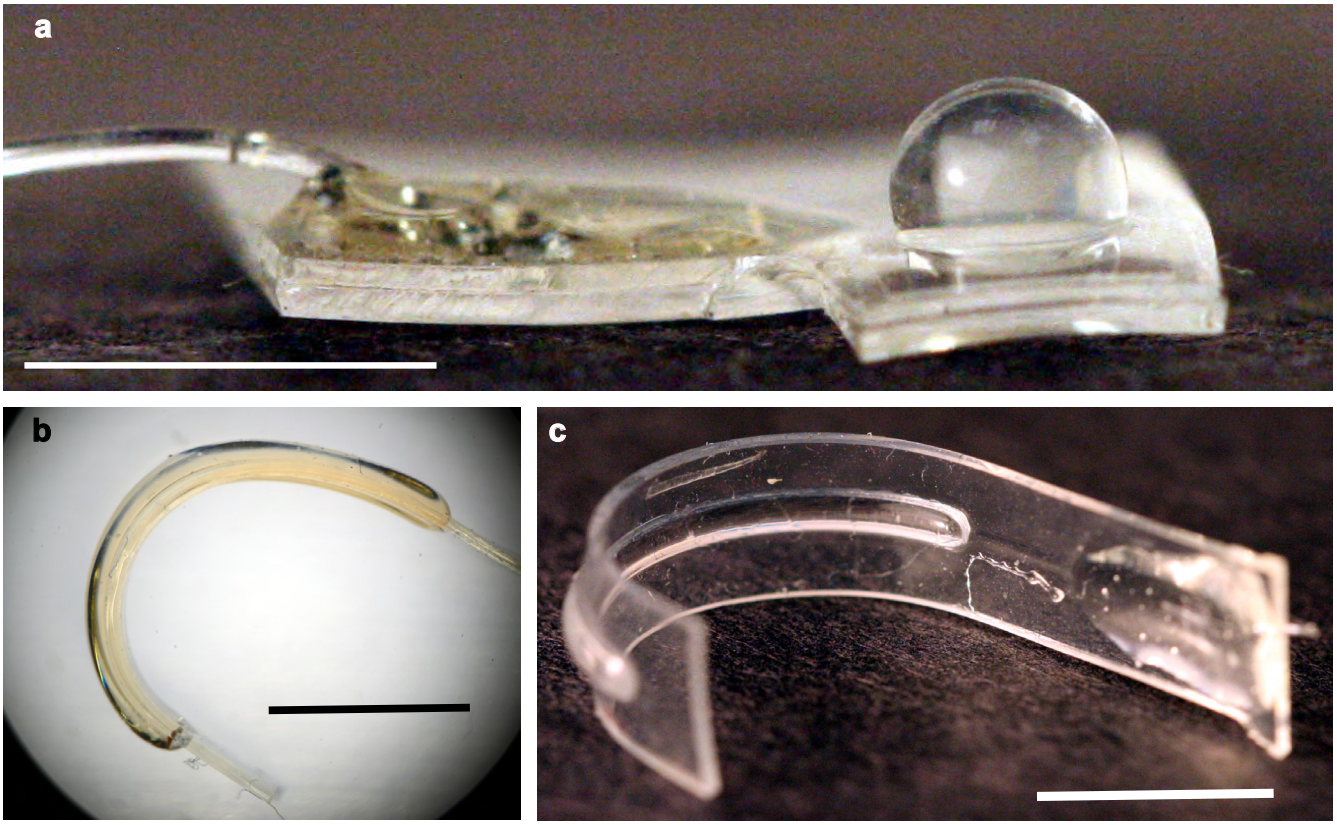

Figure S3. Injection and self–folding into soft micro–actuators with UV curable materials. a) Spherical actuator injected with UV curable silicone elastomer (Wacker Semicosil 912). b) Bending actuator injected with UV curable resin (Sartomer SR355 (90%) and Esacure KTO 46 (10%)). c) Bending actuator injected with UV curable silicone gel (Wacker SilGel 613). Scale bar is 5 mm.

the injected material, while undergoing mechanical failure, doesn't tear the silicone elastomer, we observed that the shape is preserved as the containing elastomer tends to hold the injected material in place. Indeed, the large tear strength of the elastomer selected (6.2 kN/m for the MED4-4220) resulted in a highly robust structure that was able to maintain its shape even after inducing mechanical failure of the injected material. The flexibility in material selection, provided by the proposed manufacturing paradigm, allows the user to tune the mechanical properties of the soft actuator and the mechanical interface as desired. Therefore, one could appropriately design the relative mechanical properties of the bulk material of soft actuator with respect to the properties of the injected material depending on the specific application requirements. Of course, one could imagine other working fluids that provide more exotic ways to achieve structural locking, be that chemical, electrical, or optical. Beyond that, reversible structural locking could be achieved, for example, by using water as a working fluid, and alternatively switching from freezing to melting to transform the structure between its deformed and undeformed states. When total recovery of the initial configuration is required, simply using an incompressible fluid (such as water) and closing an input valve would be a viable option.

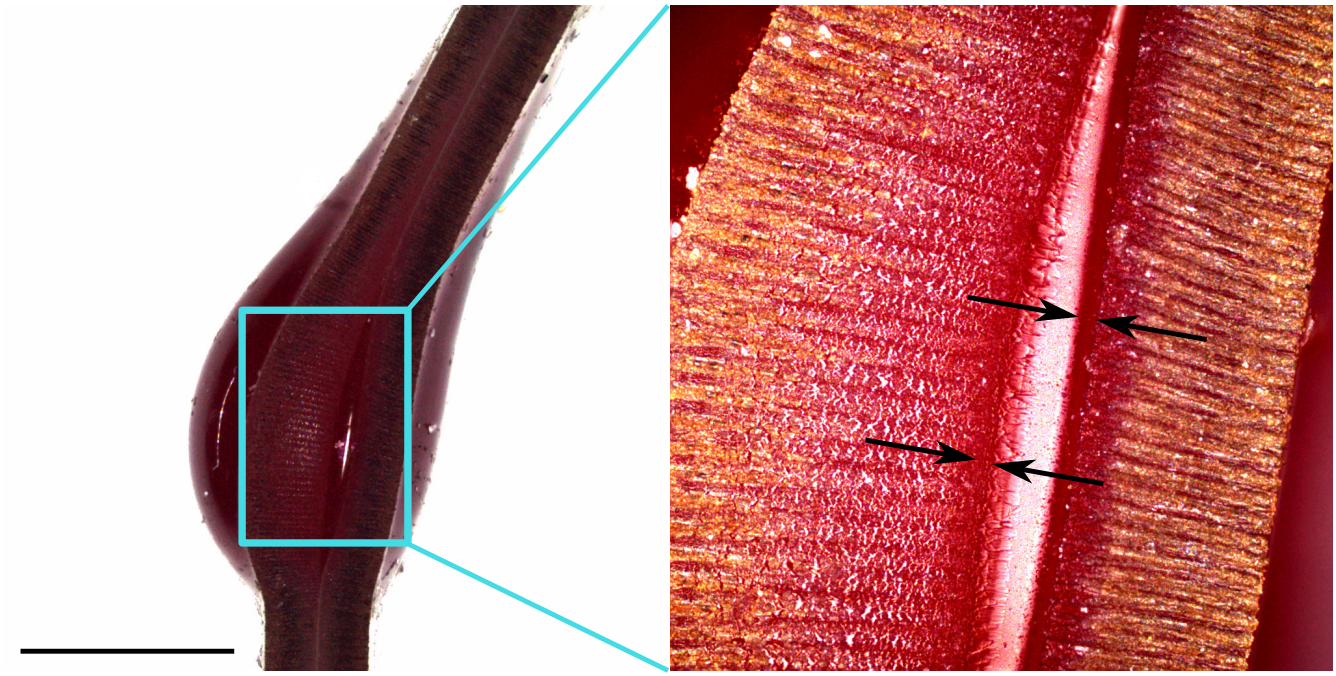

Figure S4. Injection self–folding into soft micro–actuators with thermally curable elastomer: bending actuator injected with Sylgard 184 which is then cured inside. On the left magnification of the interface between the two bonded layers composing the actuator, highlighting the small area of thermally damaged polymer. Scale bar is 1 mm.

In the design of the Peacock Spider inspired soft microrobot, we use phase-changing materials to create joints into the soft structure that can be actuated by antagonistic soft actuators. After using phase-changing materials to lock the deformed geometry, the mechanical properties will change because of the composite resulting from the injection and subsequent curing of the phase-changing material. The actuators are designed to provide a discrete bending behavior as discussed in the following section and shown in Figure S7a. We can estimate the mechanical properties of the actuator before and after the injection of the different materials tested using standard models (Voigt and Reuss) for computing Young's Modulus in composites ([12,13]). Based on the mechanical properties of the bulk materials and the injected materials (see Tables S2 and S3), we estimated the

Figure S5. Spider leg sublaminates with structural degrees of freedom injected with UV curable resin. Scale bar is 10 mm.

Young's modulus of an actuator to be 1.24 MPa. After injection of curable material and induced deformation the properties of the joint that is created are different and they depend on the properties of the material injected. We estimated the stiffness to reach 22.26 MPa when the UV-curable resin is used, and 1.63 MPa when using Sylgard 184. Using softer materials, the overall stiffness can be decreased to 0.75 MPa or 0.74 MPa by using the UV curable silicone gels SilGel 613 and Semicosil 912 respectively. We also conducted experimental tests to validate these results. Each actuator was positioned and clamped with the base fully constrained. We then imposed a force of 0.5 N using an Instron materials testing machine while recording the displacement. Subsequently, we derived the experimental Young's modulus using standard beam theory. Results showed a Young's modulus of 1.32 MPa $\pm$ 0.37 for the actuator (not injected), 22.85 MPa $\pm$ 2.55 when injected with the UV–curable resin, 1.56 MPa $\pm$ 0.62 after injection with Sylgard 184, 0.69 MPa $\pm$ 0.42 when injected with Silgel 613, and 0.65 MPa $\pm$ 0.39 with Semicosil 912. Results above represent the mean value and one standard deviation computed on two prototypes, tested three times each.

Stress release could affect the stability of the shape with time (fixing ratio). Such a phenomenon will depend on the properties of the material, thus the choice of a suitable material is of the utmost importance. We did not observe relevant changes in the geometry, after almost one year, either in the UV cured material in Figure S5, in the PDMS of Figure S4, or in any of the actuators of Figure S3. However, using materials that exhibit strain relaxation processes will result in a temporal evolution of the 3D shape driven by such relaxation. This phenomenon would likely be further amplified by the relative properties of the injected material with respect to the elastomer where the material is injected.

Design of the Peacock Spider Inspired Soft Microrobot

The spider is defined by three main sublaminate: legs, head and eyes, and abdomen.

The legs sublaminate

For creating the spider legs, we prepare a soft layer with embossed actuators (through soft lithography) positioned where the spider legs will be. The path defining the spider legs is created through precision laser micromachining, which allows us to release the legs from the elastomeric matrix so that they can be independently actuated. The leg sublaminate consists of three layers; the top and bottom layers contain embossed features, while the middle layer is unpatterned, serving as a backing for the features on the adjacent layers. Leg actuators are trapezoidal to promote discrete, joint-like bending, as opposed to the standard rectangular actuators that exhibit continuous bending (see below for more details). The spider starts from the flat configuration (Figure 3a), the four structural DoFs of the legs sublaminate (hips, left and right side knees, and chelicerae) are then injected (Figure 3b) to create the 3D structure. In Figure 3a, we show details of the working principle of the legs actuation, where the

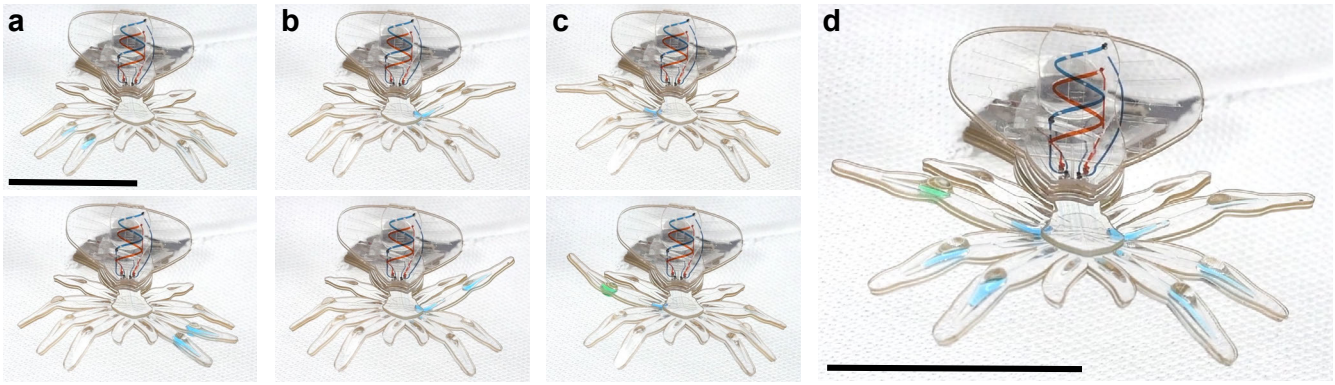

Figure S6. Actuation sequence of the six DoFs of the spider legs sublaminate. Scale bar is 10 mm.

kinematics of the structure are defined by the structural DoFs that generate the joints on the legs of the spider. Those joints are then actuated by pressurizing the actuation DoFs with blue dyed water for better visualization.

After locking the structural DoFs, we create links and joints in the soft structure which can be moved through six independent actuation DoFs of the legs sublaminate, as shown in (Figure S6) and in movie S2. Blue dyes are used to distinguish actuation from structural DoFs. The actuators are arranged in a symmetric way on the left and right side of the spider and they are manually pressurized with syringes. First, the knee joints of the two front legs are injected, independently and one at a time (shown in top and bottom of Figure S6). Subsequently, the back legs are actuated by pressurizing two different joints each (hips and knees), independently (Figure S6, b and c). Furthermore, we demonstrate multiple actuation DoFs simultaneously activated in Figure S6 d.

The head and eyes sublaminate

The inflation of the head and subsequent injection of the eyes is shown in Figure 2b and in Figure 3 c in the main text. This sublaminate also demonstrates the implementation of a colored working fluid. When fabricating this layer, selective masking was used during plasma treatment to bond only the desired regions (due to the smaller area of the head with respect to the leg sublaminate). Selective masking is used extensively in not just the head layer, but in many of the 12 layers of the full device.

The abdomen sublaminate

The abdomen sublaminate highlights multiple functionalities, including multi-layer fluid handling of a microfluidic circuit, different colored fluid patterns, and coordinated bending actuation that results in a structure with negative Gaussian curvature. In this structure, we also demonstrate the use of laser cutting on top of channels embossed in the soft layers to allow flow across the laminate. We use a small decoupling layer to isolate this sublaminate from the rest of the assembly, thus separating its motion from the other DoFs, increasing modularity, and improving manufacturing yield. All channels are bonded to the body of the spider and from that layer the fluid passes through the decoupling layer to reach the different features of the abdomen.

An abdomen sublaminate is shown in Figure 2c, with an inset highlighting the alignment between the seven layers composing it; the circles are the laser cut vias that allow the flow through the layers. We also show the abdomen elevation DoF (Figure 3d), coloring the two patterns that create the DNA symbol (Figure 3e), and actuating both the flexing actuators (Figure 3f).

The abdomen sublaminate is a seven-layer structure where all input channels are located in the bottom-most layer and fluidic lines are routed across the laminate to reach the desired layer. All lines pass through a small decoupling layer that separates the motion of the bottom layers with respect to the top-most ones. As shown in the Movie S3, Figure 3, and Figure S6, we are able to move the upper part of the abdomen independently from the rest of the body of the spider and still functionally access the microchannels (DNA symbol) on top of the actuators. This feature can pave the way towards microfluidic circuitry embedded within or on top of dynamically changing and deformable soft structures, creating new opportunities in microfluidics and soft robotics.

Design of the soft micro–actuators

Soft micro-actuators fabricated with soft lithography have been proposed by several research groups, primarily focusing on modeling, design, and extensive experimental characterization[2,14–21]. In this work, we highlight how the proposed manufacturing paradigm can expand the design freedom by combining soft lithographic techniques with precision laser micro-machining. This increase in the design space can be obtained either by changing the design on the SU-8 mold, e.g., decreasing the radius of curvature of a bending actuator (see Figure S7), or exploiting the laser cutting phase to control the bending plane of the actuator, as in Figure 1j,k (see section "Characterization of bending modes").

In the proposed MORPH system, we designed two types of soft micro–actuators: continuous bending actuators (CBAs), and discrete bending actuators (DBAs). CBAs have a rectangular shaped chamber, thus upon pressurization the loading profile along the x direction will be uniform, leading to a continuous bending behavior (Fig. S7b). In order to obtain a discrete, joint–like bending, we designed trapezoidal chambers; in this case, upon pressurizations, the load distribution will present the profile shown in Fig. S7a. Indeed the area of membrane under pressure will decrease going from the larger base to the smaller base of the trapezoid. If we assume that the pressure will uniformly distribute in the chamber and considering that $P = F/A$ the force will be larger at the larger base. This will result in an anisotropic deformation of the actuator, presenting a discrete, joint–like bending behavior (Fig. S7a). DBAs are employed in the structural and actuation DoFs of the legs, whereas the jaws, and abdomen elevating and flexing actuators are CBAs.

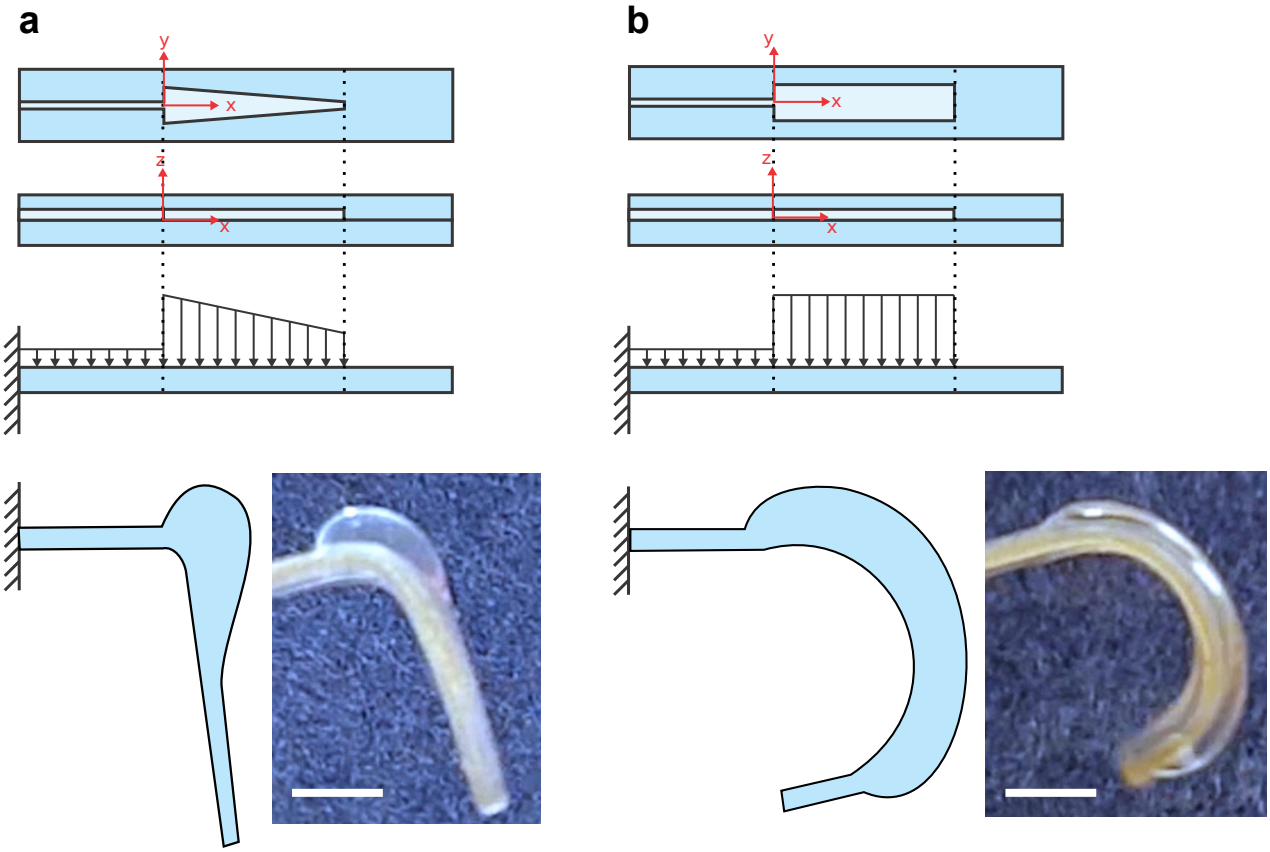

Figure S7. Continuous bending actuators (CBAs) and discrete bending actuators (DBAs). a) Top and side view of a DBA, loading profile on the actuator when pressurized, drawing of the deformed shape and picture of an actual prototype. b) Top and side views of a CBA, scheme of the loading profile when pressure is applied, and drawing of the deformed state compared with an actual prototype. Scale bar is 1 mm.

Assembly Procedure

The peacock spider–inspired MORPH system is composed of 12 soft layers. Here, we distinguish between two sublaminates (each composed of six soft layers): the body sublaminate (Figure S8), composed of the legs sublaminate and head and eyes, and the abdomen sublaminate (Figure S9). Each soft layer is individually manufactured using soft lithography and the thermally cured silicone elastomer is peeled off from the SU-8 patterned silicon wafer using an adhesive substrate or carrier. The substrate consists of a Gel-Pak 8 film, Gel-Pak®, a flexible but not stretchable substrate material with a tacky surface to hold the layers during processing and/or assembly. Each layer is then covered with a transparent layer of polyester film (3.6 μm Mylar®, Chemplex Industries, Inc.) to preserve cleanliness during laser machining and protect the silicone elastomer for storage. Subsequently, the elastomer is cut using a precision laser micromachining system according to a specific design pattern after alignment to fiducials defined during soft lithography. Alignment holes are laser cut through the carrier to be used for future pin alignment. The protective polyester film is removed right before the plasma treatment phase to expose the soft layer,

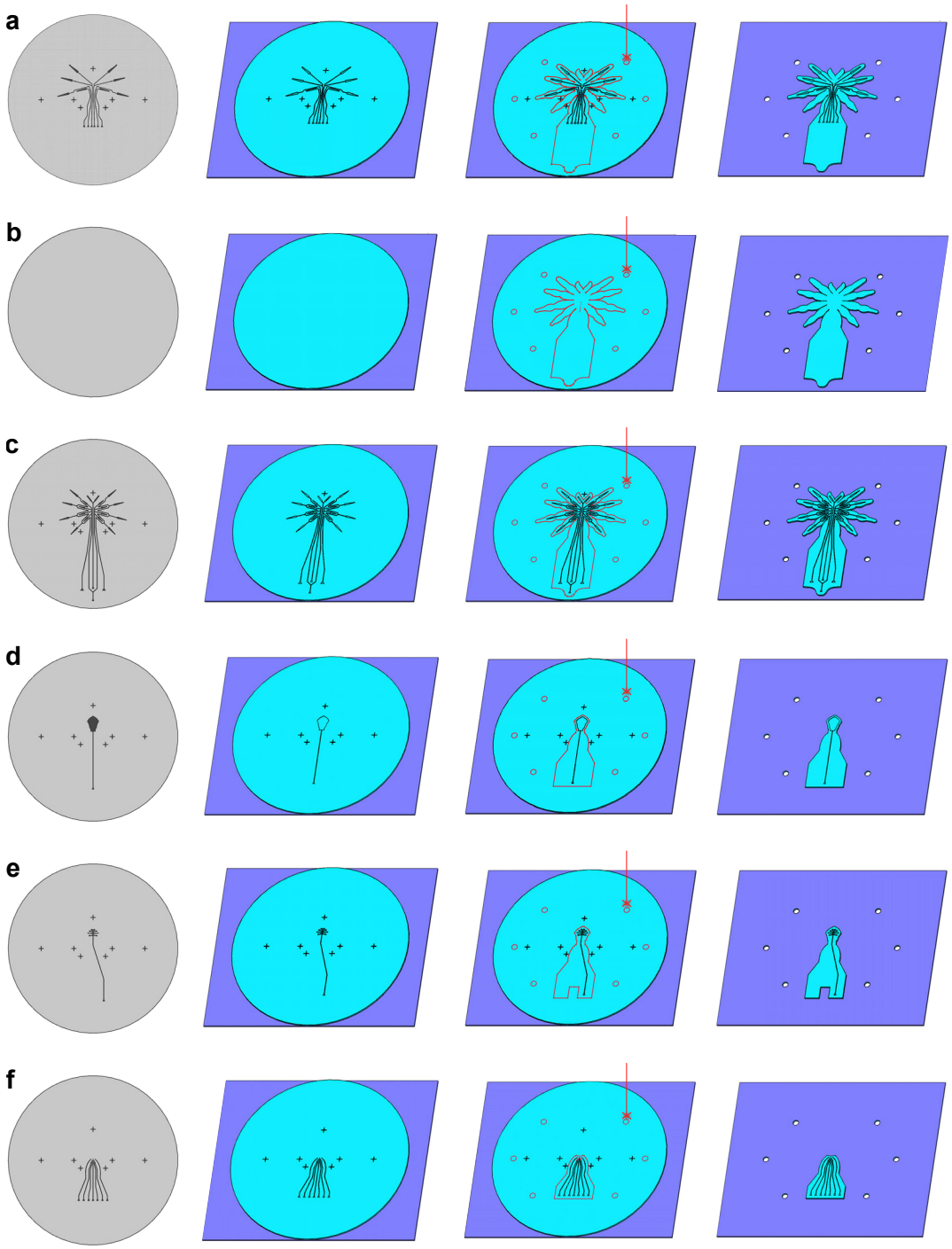

Figure S8. Fabrication process of the soft layers for the spider body sublaminate. For each layer: a) legs structural, b) legs blank, c) legs actuation, d) head, e) eyes, and f) piping, four fabrication steps are shown (SU-8 patterned wafer mold, peel-off and preparation of sample, laser machining, and scrap removal and preparation for plasma treatment).

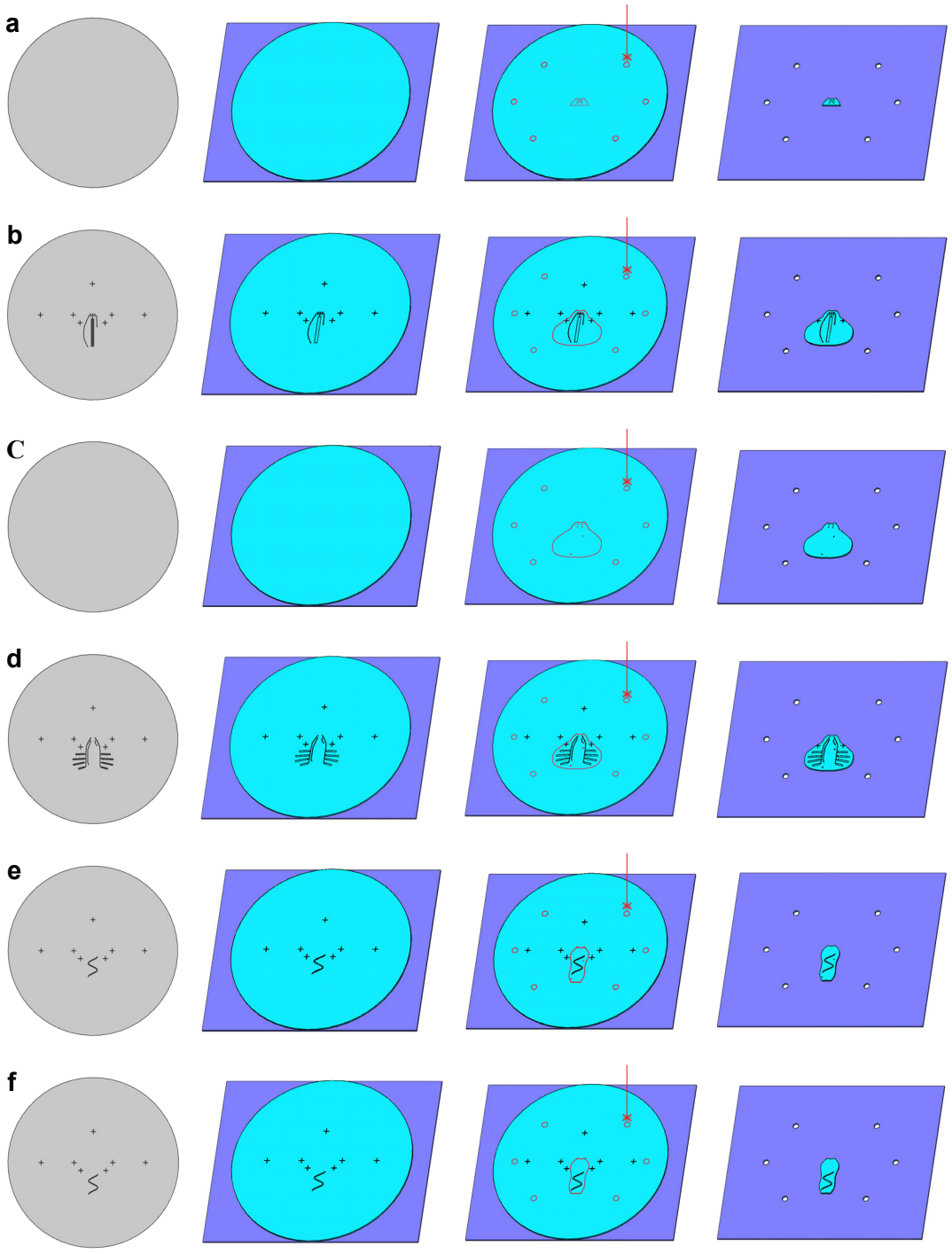

Figure S9. Fabrication process of the soft layers for the spider abdomen sublaminate. For each layer: a) decoupling, b) abdomen elevating actuator, c) abdomen blank, d) abdomen flexing actuator, e) DNA strand 1, and f) DNA strand 2, four fabrication steps are shown (SU-8 patterned wafer mold, peel-off and preparation of sample, laser machining, and scrap removal and preparation for plasma treatment).

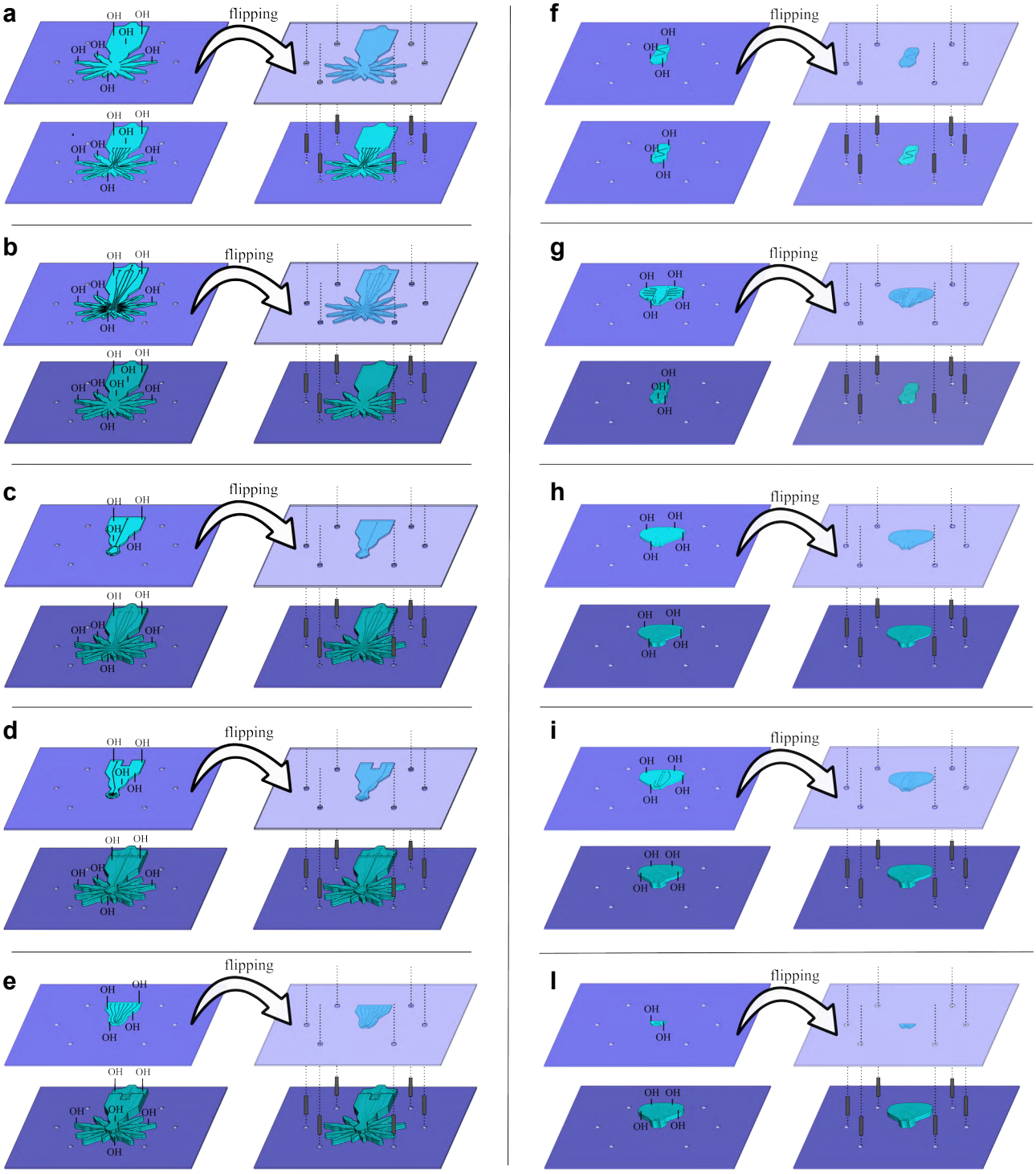

Figure S10. Spider assembly sequence. For each sub-figure, oxygen plasma functionalization, realignment through precision dowel pins, and chemical bonding are illustrated. a)–e) are the assembly steps of the body sublaminate, f)–l) is the assembly sequence for the abdomen.

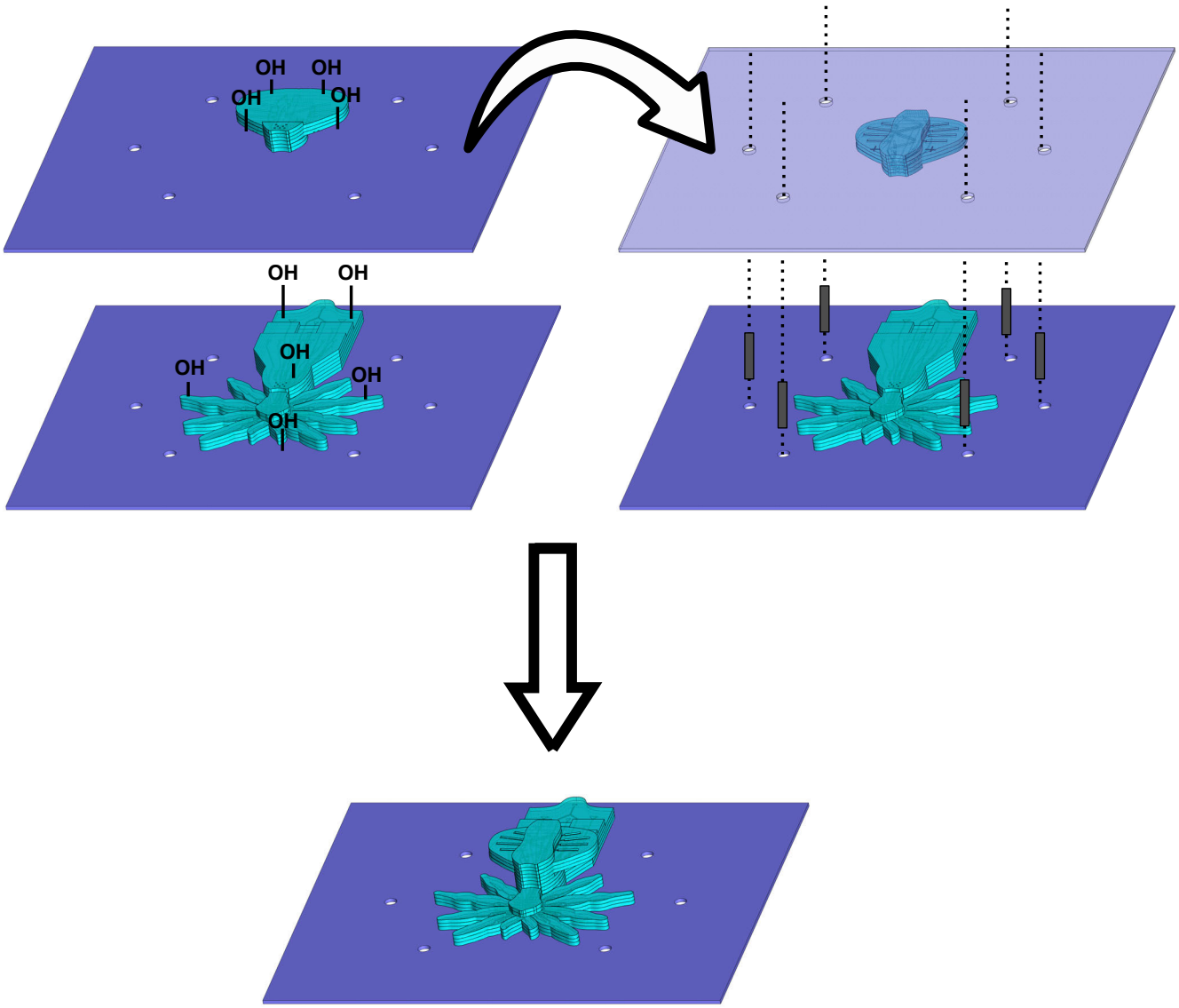

Figure S11. Assembly of the body sublaminate with the abdomen sublaminate using oxygen plasma treatment.

achieve chemical surface functionalization, and bonding. Layers are realigned and bonded together using O_2 plasma (35 W for 30 s) treatment (Pico BR PCCE 7", Diener electronic GmbH + Co. KG). The bonding sequence for the peacock spider is illustrated in Figure S10. For the body of the spider (Figure S10, a–e), the bottommost is the legs actuation layer that is assembled together with the legs blank layer (Figure S10a). Subsequently, legs structural (Figure S10b), head (Figure S10c), eyes (Figure S10d), and piping layers (Figure S10e) will follow. As regards the abdomen (Fig. S10, f–l), the topmost is the DNA strand layer that is assembled together with another DNA strand layer (Figure S10f) to form a double DNA helix (logo of the Wyss Institute for Biologically Inspired Engineering). Subsequently, abdomen flexing actuator (Figure S10g), abdomen blank (Figure S10h), abdomen elevating actuator (Figure S10i), and decoupling layers (Figure S10l) will follow. As a last step, the body and abdomen sublaminates are assembled together following the same procedure described above (Figure S11). The spider is designed with a modular approach so that the two sublaminates can be assembled separately and then bonded together at the end to ease the fabrication process and guarantee a higher manufacturing yield.

Structural DoF are obtained by injecting UV-curable resin (SR-355, di-trimethylolpropane tetraacrylate, Sartomer) mixed with a photoinitiator (Esacure KTO 46, Lamberti SpA). UV exposure is performed with a UV Exposer (OAI Model 30 UV Light Source), with a measured exposure power of 19.5 mW/cm^2 at 365 nm.

Characterization of bending modes

We explored a new mode of actuation for elastomeric structures where we use the laser cut path to define the motion of actuatable sections of a soft structure (i.e. a soft actuator). In the main text we introduced the concept of *out-of-plane bending*, as the soft actuator bends out of the plane of its defining geometry, and of *in-plane bending*, as the bending deformation is entirely within the plane of the actuator. As detailed in the main text, we demonstrate that we are able to define the motion plane of soft micro-actuators by changing the wall thickness by means of precise laser machining. A soft actuator will bend *out-of-plane* if the membrane thickness m is the smallest dimension (i.e., smaller than the adjacent wall thickness d). This behavior remains dominant until the minimum cut distance d becomes similar in magnitude to the membrane thickness m. When $d \approx m$, the bending axis begins to rotate, as m is no longer the actuator's smallest dimension. Further decreasing the minimum cut distance below the membrane thickness causes the bending axis to rotate further, until d is appreciably smaller than m and actuator will bend *in-plane*. The cut distance on the other side of the actuator matters only in that we ensure its thickness is much greater than d (in the same way that we must ensure that the bottom of the actuator is much thicker than the membrane m).

To quantify this behavior, we performed visual tracking of various actuators. The actuators are manufactured using the

same procedure as for the soft layers composing the spider. We fabricated actuators with minimum cut distances ranging from three times the membrane thickness down to the smallest distance we could fabricate successfully (determined in part by thermal damage effects, discussed below). The final bend angle is defined as the inverse tangent of the deflection along the z-axis with respect to deflection along the y-axis (Figure 1j, k). As such, a typical out-of-plane bending actuator (i.e., one that bends entirely about the y-axis) would have a bend angle of 90°. Similarly, an actuator that demonstrates fully in-plane bending (i.e., one that bends entirely about the z-axis) would have a bend angle of 0°. The data in Figure 2 k show that indeed there is a transition from out-of-plane bending to in-plane bending as the minimum cut distance approaches and subsequently passes below the membrane thickness. The spread in the experimental data is due to experimental and fabrication errors.

We first fabricated actuators with minimum cut path distances in the range of about 40 μm (the minimum distance we could reliably cut, as detailed in the thermal damage analysis, below) to about 440 μm, all with a membrane thickness of approximately 150 μm (formally, 146 μm mean with a standard deviation of 8.4 μm, n = 24). To test an actuator, we secured it to a custom–made fixture, positioning the actuator as a cantilever beam. After pneumatically pressurizing the actuator to a set value (70 kPa) as determined by an integrated digital pressure gauge (BSP000W, Balluff Inc.), we used a syringe pump (Pump 11 Elite, Harvard Apparatus) to deliver a known volume of additional air (10 ml at a rate of 25 ml/min). With a pair of high–speed cameras (Phantom v7.3, Vision Research Inc.) arranged orthogonally, we visually tracked the tip position of the actuator as it deformed. The three-dimensional path of the tip of the actuator was reconstructed using a custom MATLAB (v. R2017a, MathWorks Inc.) script that relied in part on motion analysis software (ProAnalyst, Xcitex Inc.). The output of the reconstruction was the entire XYZ position history of the tip of the actuator, with corresponding pressure values.

It is interesting to note that the data are quite spread within the transition region from out-of-plane to in-plane bending. We hypothesize that, in addition to material irregularities and manufacturing imperfections, some of the spread may be attributed simply to the hyperelastic nature of the material. As the actuator is pressurized, the thinnest portion (whether that is the membrane defined lithographically or the sidewall defined by laser cutting) will expand to a much larger degree than the rest of the actuator. When the minimum cut path distance is of similar magnitude to the membrane thickness, we observe complex, hybrid motions in which an actuator will transition from one bending mode to another throughout the course of a single inflation (Movie S4). We believe this behavior is due to a strain stiffening effect, wherein the elastic modulus increases with deformation. As such, it is not only the geometry of the actuator but also the time-varying mechanical properties of the material that influences bending motion.

Movie S1

This movie shows the entire sequence of injection of the structural DoFs of the peacock spider and coloring DoF of the eyes. A three dimensional soft micro structure emerges from the injection of a phase-changing material in the hips, knees, jaws, and head of the spider. The hips consist of eight interconnected actuators (one for each leg) that bend all the legs of the spider downwards upon pressurization simultaneously. The knees (one for each leg) are independently controlled on the left and right side (four for each side). Upon inflation, they bend the legs further down, creating a second joint. Two jaws are interconnected and inflate at the same time. The head is the last structural DoF and it consists of a single independent actuator. After the three dimensionality is locked by exploiting the properties of the phase-changing material (i.e. UV exposure), coloring DoF is demonstrated by injecting the eyes of the spider with dyed water.

Movie S2

This movie focuses on the abdomen sublaminate showing the entire sequence of injection of the actuation DoFs and coloring DoFs. After the three dimensionality of the spider is locked by exploiting the properties of the phase-changing material (i.e. UV exposure), actuation DoFs are demonstrated. The abdomen elevating actuator is inflated to raise the abdomen with respect to the rest of the body. Coloring DoF are shown by injecting dyed water in the two DNA strands on top of the abdomen. Finally, the flexing actuators of the abdomen are pressurized to move the structure outwards. The last part of the video shows multiple DoFs in action (from abdomen and body sublaminates).

Movie S3

This movie shows the actuation DoFs of the legs of the spider and coloring DoFs of the abdomen sublaminate.

After locking the structural DoFs, six independent legs actuation DoFs are demonstrated sequentially. First, the back legs are actuated by pressurizing two different joints each (hips and knees), independently. Subsequently, the knee joints of the two front legs are injected. Dyes are used to distinguish antagonistic actuation from structural DoFs. Then, all the legs actuation DoFs are pressurized simultaneously and in a random sequence. A couple of close–up views of the antagonistic leg actuation mechanism are also shown in the front legs of the spider.

After inflation of the abdomen elevating actuator (to raise the abdomen with respect to the rest of the body), changing colored fluid patterns are shown flowing in the abdomen double DNA helix. The microfluidic circuit of the DNA pattern (Fig. 1i) is open and double–ended so that dyed water can recirculate from the piping layer (Fig. S8f) through the decoupling layer, (Fig. S9a) up to the DNA strands layers (Fig. S9, e and f). The two DNA strands are initially red and blue, then the

sequence of coloring changes to: red and orange, green and orange, and green and dark purple.

Movie S4

In this video we show top and side view of different soft micro–actuators. The first one is a DBA bending out-of-plane. The second part of the video shows an entirely in-plane actuator, followed by a close up view of the chamber during inflation. The last part of the video shows a DBA with a behavior in between out-of-plane and in-plane.

Movie S5

In this video we demonstrate the injection-induced self–folding with a phase–changing material (UV curable resin) to transform actuators into structural elements. After exposure to UV light, pipes are cut and the two–dimensional laminate is effectively transformed into a three–dimensional soft structure. This process is demonstrated in the video on half of the spider body to ease the visualization of the arising three–dimensional shape.

Movie S6

The structural DoFs of the legs sublaminate have been previously injected with UV curable resin and the video shows subsequent pressurization of the actuation DoFs to move the joints created during the injection-induced self–folding process. Actuation is performed with red dyed water.

References

1. Liu, Y., Genzer, J. & Dickey, M. D. "2D or not 2D": Shape-programming polymer sheets. Prog. Polym. Sci. **52**, 79–106 (2016). URL http://linkinghub.elsevier.com/retrieve/pii/S0079670015001021http://dx.doi.org/10.1016/j.progpolymsci.2015.09.001. DOI 10.1016/j.progpolymsci.2015.09.001.

2. Russo, S., Ranzani, T., Walsh, C. J. & Wood, R. J. An Additive Millimeter-Scale Fabrication Method for Soft Biocompatible Actuators and Sensors. Adv. Mater. Technol. 1700135 (2017). URL http://doi.wiley.com/10.1002/admt.201700135. DOI 10.1002/admt.201700135.

3. Ma, K. Y., Chirarattananon, P., Fuller, S. B. & Wood, R. J. Controlled Flight of a Biologically Inspired, Insect-Scale Robot. Sci. **340**, 603–607 (2013). URL http://www.sciencemag.org/cgi/doi/10.1126/science.1231806. DOI 10.1126/science.1231806.

4. Zhao, W. Interactive Robogami. Ph.D. thesis, Massachusetts Institute of Technology (2015). URL https://dspace.mit.edu/handle/1721.1/100861.

5. Qin, D., Xia, Y. & Whitesides, G. M. Soft lithography for micro- and nanoscale patterning. Nat. Protoc. **5** (2010). DOI 10.1038/nprot.2009.234.

6. Unger, M. a., Chou, H. P., Thorsen, T., Scherer, a. & Quake, S. R. Monolithic microfabricated valves and pumps by multilayer soft lithography. Sci. (New York, N.Y.) **288**, 113–116 (2000). DOI 10.1126/science.288.5463.113.

7. Aukes, D. M., Goldberg, B., Cutkosky, M. R. & Wood, R. J. An analytic framework for developing inherently-manufacturable pop-up laminate devices. Smart Mater. Struct. **23**, 094013 (2014). URL http://stacks.iop.org/0964-1726/23/i=9/a=094013?key=crossref.eabf1f6b53b24c7890e5eb1c0d94ab21. DOI 10.1088/0964-1726/23/9/094013.

8. Safranski, D. L. & Gall, K. Effect of chemical structure and crosslinking density on the thermo-mechanical properties and toughness of (meth)acrylate shape memory polymer networks. Polym. **49**, 4446–4455 (2008). URL https://www.sciencedirect.com/science/article/pii/S0032386108006551. DOI 10.1016/J.POLYMER.2008.07.060.

9. Johnston, I. D., McCluskey, D. K., Tan, C. K. L. & Tracey, M. C. Mechanical characterization of bulk Sylgard 184 for microfluidics and microengineering. J. Micromechanics Microengineering **24**, 35017 (2014). URL http://stacks.iop.org/0960-1317/24/i=3/a=035017. DOI 10.1088/0960-1317/24/3/035017.

10. Wacker. Silicone Gel Solutions. Tech. Rep. (2011). URL https://www.wacker.com/cms/media/publications/downloads/6982_EN.pdf.

11. Wacker. Wacker silgel® 612 a/b. Tech. Rep. (2008). URL https://www.swiss-composite.ch/pdf/t--Silgel-612.pdf.

12. Watt, J. P., Davies, G. F. & O'Connell, R. J. The elastic properties of composite materials. Rev. Geophys. **14**, 541 (1976). URL http://doi.wiley.com/10.1029/RG014i004p00541. DOI 10.1029/RG014i004p00541.

13. Mayer, G. & Sarikaya, M. Rigid biological composite materials: Structural examples for biomimetic design. Exp. Mech. **42**, 395–403 (2002). URL http://link.springer.com/10.1007/BF02412144. DOI 10.1007/BF02412144.

14. Morimoto, K., Utsumi, A. & Konishi, S. A design of longitudinally-divided balloon structure in PDMS pneumatic balloon actuator based on FEM simulations. 16th Int. Conf. Solid-State Sensors, Actuators, Microsystems 2774–2777 (2011). URL http://ieeexplore.ieee.org/xpls/abs%7B_%7Dall.jsp?arnumber=5969597http://ieeexplore.ieee.org/xpls/abs_all.jsp?arnumber=5969597.

15. Paek, J., Cho, I. & Kim, J. Microrobotic tentacles with spiral bending capability based on shape-engineered elastomeric microtubes. Sci. Reports **5**, 10768 (2015). URL http://www.nature.com/doifinder/10.1038/srep10768. DOI 10.1038/srep10768.

16. Wakimoto, S., Suzumori, K. & Ogura, K. Miniature Pneumatic Curling Rubber Actuator Generating Bidirectional Motion with One Air-Supply Tube. Adv. Robotics **25**, 1311–1330 (2011). URL http://www.tandfonline.com/doi/abs/10.1163/016918611X574731. DOI 10.1163/016918611X574731.

17. De Volder, M. & Reynaerts, D. Pneumatic and hydraulic microactuators: a review. J. Micromechanics Microengineering **20**, 043001 (2010). URL http://stacks.iop.org/0960-1317/20/i=4/a=043001http://stacks.iop.org/0960-1317/20/i=4/a=043001?key=crossref.13b731aac4d13755bb3cfe368f346906. DOI 10.1088/0960-1317/20/4/043001.

18. Gorissen, B., De Volder, M., De Greef, A. & Reynaerts, D. Theoretical and experimental analysis of pneumatic balloon microactuators. Sensors Actuators A: Phys. **168**, 58–65 (2011). URL http://linkinghub.elsevier.com/retrieve/pii/S0924424711002275. DOI 10.1016/j.sna.2011.03.057.

19. Gorissen, B., Vincentie, W., Al-Bender, F., Reynaerts, D. & De Volder, M. Modeling and bonding-free fabrication of flexible fluidic microactuators with a bending motion. J. Micromechanics Microengineering **23**, 045012 (2013). URL http://stacks.iop.org/0960-1317/23/i=4/a=045012?key=crossref.f68b933e55424a3a92ba998f4d298e3b. DOI 10.1088/0960-1317/23/4/045012.

20. Gorissen, B. et al. Elastic Inflatable Actuators for Soft Robotic Applications. Adv. Mater. 1604977 (2017). URL http://doi.wiley.com/10.1002/adma.201604977. DOI 10.1002/adma.201604977.

21. Liang, X., Sun, Y. & Ren, H. A Flexible Fabrication Approach towards the Shape Engineering of Microscale Soft Pneumatic Actuators. IEEE Robotics Autom. Lett. **3766**, 1 (2016). URL http://ieeexplore.ieee.org/lpdocs/epic03/wrapper.htm?arnumber=7500037. DOI 10.1109/LRA.2016.2585298.